Measurements of polyatomic molecule formation on an icy grain analog using fast atoms

S. Madzunkov,[1] B. J. Shortt,[2] J. A. MacAskill,[1] M. R. Darrach,[1] and A. Chutjian[1]

[1]*Atomic and Molecular Collisions Group, Jet Propulsion Laboratory, California Institute of Technology,*
Pasadena, California 91109, USA

[2]*Department of Applied Physics and Instrumentation, Cork Institute of Technology, Cork, Ireland*

Measurements are reported for production of CO_2 resulting from the impact of a monoenergetic $O(^3P)$ beam upon a surface cooled to 4.8 K and covered with a CO ice. Using temperature-programmed desorption and mass spectrometer detection, one clearly detects increasing amounts of CO_2 formation with $O(^3P)$ energies of 2, 5, 10, and 14 eV. This is a measurement of polyatomic molecule formation on a surface in a new regime using superthermal atoms. The chosen surface coverage, surface temperature, and superthermal atom energy simulate conditions in shock-heated circumstellar and interstellar regions.

PACS number(s): 34.50.Dy, 98.58.Bz

Dust, ices, and surfaces of planets, comets, and asteroids play an indispensable role in the chemical evolution of the protostellar regions and the interstellar medium (ISM), from the catalytic production of molecular hydrogen to the formation of organics (CH_3OH, H_2CO, CH_4, NH_3, CN-bonded species, etc.) critical to the origin of life. Laboratory studies of ices and dust grain analogs are crucial to defining and constraining the environmental conditions in dense and dusty clouds. Grain-particle interactions include effects of ion and neutral atomic fluxes, UV radiation intensity, cosmic-ray intensity, and surface temperature. A wide range of laboratory studies has been carried out on the effects of ion irradiation [1–4]; the UV photolysis of molecules (including amino acids) on icy grain analogs [5–7]; thermal-energy atomic irradiation by oxygen atoms in both a spray [8] and directed-beam [9,10] geometry; and on the thermal desorption characteristics of molecules from analogs of icy dust grains [11]. Closer to home, the area of superthermal atom-gas and atom-surface collisions has important bearing on surface catalysis, etching, manufacture of polymeric materials, atmospheric chemistry, and low-earth orbit erosion [12–14]. In all cases, one requires a detailed understanding of the atom-gas reaction channels that become open at the higher collision energies.

Fast neutral species such as H, He, O, OH, CO, and H_2O are present in the circumstellar regions and the ISM by virtue of energetic processes such as stellar outflows, shocks, dissociation and ionization of gas-phase particles by stellar UV photons, and the charge exchange of outgoing stellar wind ions with circumstellar neutral clouds. Neutral-neutral reactions almost certainly play a major role within cold dark clouds where UV penetration is blocked by dust, and in hot molecular cores where shock heating of neutral atomic species can occur [15]. The clearest example of the importance of neutral-neutral reactions is the astrophysical observation that abundant CO_2 is detected in a quiescent dark cloud (Elias 16), where no sources of UV radiation are present, and hence where photochemistry cannot have a role [16]. Whittet *et al.* [16] and Orient *et al.* [17] have performed studies on the effects of fast atomic collisions with surface-adsorbed molecules. There, measurements were made of optical emissions from electronically excited CO_2^* and NO_2^* produced

via reactions $O+CO+surface \rightarrow CO_2^*$ and $O+NO+surface \rightarrow NO_2^*$ in the presence of surfaces at temperatures of 245–345 K (to simulate low-earth orbit interactions), and at moderate vacua of 10^{-5} Pa. Due to experimental constraints at that time it was not possible to freeze target gases onto a surface, or to detect directly the collision products by temperature-programmed desorption (TPD) and mass spectrometry under ultrahigh vacuum conditions.

Neutral atomic beams, free of other species (e.g., fragments from the feed material), and of known quantum state, energy, and energy width are difficult to generate in the laboratory. The fast-atom apparatus used herein is the only source capable of generating solely ground-state $O(^3P)$ oxygen atoms at energies in excess of 1 eV, with no admixture of other atoms or molecules. A schematic diagram of the apparatus is shown in Fig. 1, and details of its operation are given here and in Ref. [18]. This apparatus was significantly modified by the addition of a quadrupole mass spectrometer (MS), a surface target coupled to a liquid helium (LHe) refrigerator, a translation stage to move the surface target from the exposure region to the field of view of the MS electron impact ionizer, and an automated TPD system for heating the cold surface and recording simultaneous mass spectra for, in this case, up to eight desorbed species.

A schematic diagram of the fast-atom apparatus is given in Fig. 1. A 500-μA current of electrons is generated from a hairpin tungsten filament F. confined by a 6-T solenoidal field, and accelerated to 11 eV. The beam is directed across a gas nozzle G where O^- ions (energies less than 1 eV) are formed by dissociative attachment to the CO feed gas according to the reaction $e+CO \rightarrow C(^3P, ^1D)+O^-(^2P)$. The confined O^- ions are extracted, separated from the electron beam, and energy analyzed by the trochoidal monochromator TM. The faster electron beam is only slightly deflected within the TM, and is collected in the Faraday cup FC_e. The monoenergetic $O^-(^2P)$ ions are accelerated to the desired final O-atom energy by a grid prior to the multiple-pass mirror box (M). Within M a portion of the O^- is converted to $O(^3P)$ through photodetachment using light L (the 514.5-nm green line) of a 10-W argon-ion laser, to form exclusively ground-state $O(^3P)$ atoms. (Note: the laser never intercepts the target
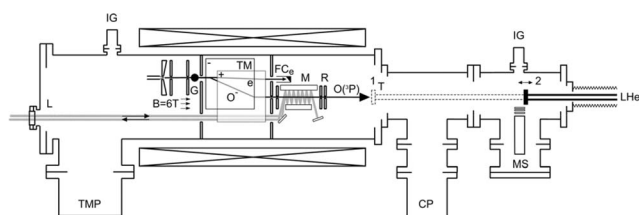
FIG. 1. Schematic diagram of the fast-atom apparatus. The legend is: photodetaching laser L, turbomolecular pump TMP, ion gauges IG, gas source G, trochoidal monochromator TM, electron Faraday cup FC_e, multiple-pass mirror box M, reflecting grids R, surface target T, cryopump CP, mass spectrometer MS, liquid helium coolant flow LHe, and the magnetic field direction and magnitude B.

surface nor participates in the surface reaction in any way.) The atomic oxygen beam continues through M, while the undetached O^- is blocked by reflecting grids R mounted at the exit of M. The electron detachment efficiency is 10–12%, as determined by measuring the change in O^- current on a mesh covering element R, with the laser "on" and "off." Pumping in the beam source region is with a 3000 l/s turbomolecular pump TMP, and in the target region with a 1000 l/s cryopump CP. Pressures in the chambers are measured with ion gauges IG.

The surface target T consists of CO frozen on a gold surface mounted to a linear translation stage. To ensure that the target is free of residual CO_2 molecules, the entire translation stage is heated to 450 K for approximately 10 min prior to each TPD run. Following bakeout, the pressure in the vicinity of the mass spectrometer is below 10^{-10} Pa, as measured by a cold cathode gauge located above position 2 (Fig. 1). A mass spectrum is recorded after each bakeout of the translation stage to determine the components of the background gas. These were found to be water, nitrogen, and trace amounts of CO_2.

In a TPD run the cleaned gold surface is translated into position 1 for deposition and bombardment. The surface is cooled to 4.8 K by a flow of liquid helium (LHe), whereupon CO is introduced into the chamber at a pressure of 10^{-3} Pa (at gas jet G) and 10^{-7} Pa (near the target T). The CO molecules are deposited onto the cold surface while the surface is simultaneously bombarded by the $O(^3P)$ ground-state beam for 1 h. The oxygen beams used in separate exposures were at energies of 2, 5, 10, and 14 eV, and at neutral currents of 10^7 atoms/s. The deposition pressure of CO in the chamber was held constant for all measurements. The base pressure in the target region was 5×10^{-10} Pa. The target was separately baffled and pumped to maintain a pressure differential during O-beam and CO operation of 10^{-5} Pa (source) and 10^{-7} Pa (target), a differential of a factor of 100.

After exposure the $O(^3P)$ beam is turned off, the surface retracted to position 2. It is then warmed to 350 K at a rate of 1.0 K/min to 100 K, and at a rate of 10 K/min from 100 to 350 K. The desorbing species are detected as a function of surface temperature with a quadrupole mass spectrometer (MS). An example of the TPD data is shown in Fig. 2 for 5-eV O-atom energy. Comparable results (not shown here) were obtained at 2, 10, and 14 eV. A personal com-
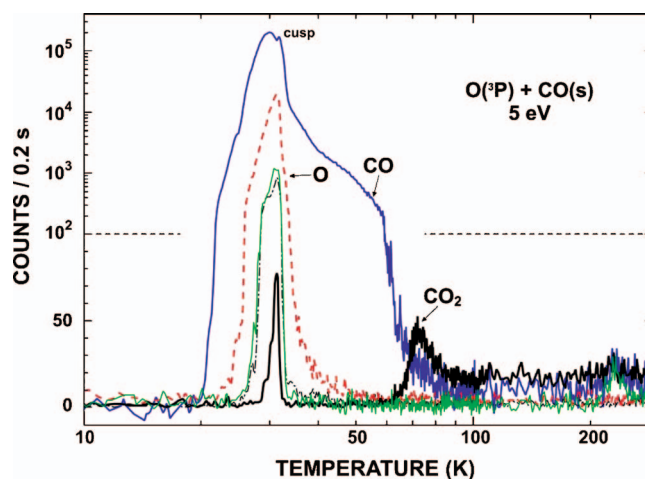

FIG. 2. (Color) TPD spectrum following the exposure to a 5-eV $O(^3P)$ beam of CO frozen on a gold substrate. The TPD consists of a low-temperature physisorbed peak (30 K), and a high temperature (70 K) chemisorbed peak consisting of only CO_2. The mass channels are ^{16}O (---- and red), $^{18}H_2O$ (— and green), ^{28}CO (— and blue), $^{32}O_2$ (--·--·- and black), and $^{44}CO_2$ (— and black). The area ratio of the two peaks comprising the cusp at 30 K is used to obtain a CO coverage of 2–3 monolayers; the peak/valley ratio of the cusp is 0.7. Note the linear scale up to 10^2, and logarithmic scale thereafter.

puter is used to monitor and record the electron beam current, target surface temperature, and the mass spectrometer signal for multiple species, while controlling the electron beam energy, electrode potentials, and the surface-target heater. The temperature ramp is sufficiently slow that multiple scans of the MS are performed at each temperature step. The MS is used in a multiple ion monitoring mode to detect the production of up to eight separate masses during the TPD ramp.

Five desorbed species are evident in Fig. 2. The strong, cusped peak at 30 K is interpreted as being due to physisorbed and chemisorbed CO ice layers, in which the bonding is due to relatively weak CO-CO intermolecular (physisorbed) and strong CO-surface (chemisorbed) potentials. Warming the surface up to the 30 K melting point of this ice mélange throws *all* the reacted and adsorbed species into the vapor phase. The ejected species are $^{18}H_2O$, ^{28}CO, $^{32}O_2$, and $^{44}CO_2$. The ^{12}C and ^{16}O arise from fractionation in the MS ionizer of H_2O, CO, O_2, and CO_2. The contribution of $^{28}N_2$ to the signal at mass 28 was negligible, as evidenced by the fact that no fractionated ^{14}N could be detected in the baseline vacuum prior to and following each TPD measurement. In addition, the detected C^+/CO^+ intensity ratio was consistent with that given by the fraction of CO alone. The source of the H_2O is trace background water in the vacuum chamber. A search was made in a separate measurement for other mass species in the range 5–50 amu, and none was found to within the system detection limit. From a mass spectral scan of the background gases, and with knowledge of the background pressure, the sensitivity of the detection system is estimated to be less than 3×10^{-11} Pa partial pressure of CO_2.

At 70 K one detects *only* desorption of CO_2 chemisorbed

to the gold substrate, and formed in the reaction $O+CO(s) \rightarrow CO_2(s)$. [Here, (s) denotes a surface-adsorbed species]. Finally, one detects at 230 K desorption of the residual H_2O background frozen on the target (Fig. 2). The CO desorption temperature range found here agrees with another study in which CO desorption was found to start at 24 K, and was complete by 33 K [19]. The behavior of the CO desorption (cusped peak at 30 K on the logarithmic scale of Fig. 2) was used to provide an estimate of the number of monolayers formed. This was done by comparing the net signal under the physisorbed feature (lower-T cusp) with that of the chemisorbed feature (higher-T cusp) [20]. This estimate gave approximately a 2–3 monolayer coverage. This is in agreement with an estimate based on the CO partial pressure, exposure time, and a unity sticking coefficient.

There is the possibility that some of the desorbed CO_2 may have arisen from gas-phase $O+CO$ collisions. Using estimates of the CO gas density (3.5×10^7 cm^{-3}), the reaction cross section (10^{-16} cm^2), and path length through the gas (12 cm), one obtains a CO_2 formation rate of 0.4/s, or a total of 1400 CO_2 molecules formed throughout a 3600-s exposure period. After desorption and electron impact ionization in the MS, this would give rise to an undetectable contribution to the surface desorbed CO_2 signal. In addition, the simple hard-sphere cross section must be an overestimate, since the intermediate CO_2 molecule must dissipate its O-CO center-of-mass collision energy *and* bond energy in order to stabilize.

A TPD normalization procedure was adopted in order to exhibit the clear enhancement of integrated TPD signals, measured for the different ion masses (^{12}C, ^{16}O, $^{18}H_2O$, ^{28}CO, $^{32}O_2$, and $^{44}CO_2$), due to O-atom exposure. The data analysis proceeds as follows. The TPD curves are recorded at four different O-beam energies E with simultaneous detection of the six masses m. Data are recorded both with and without the laser beam. For each m and laser power P one integrates the TPD signal over the temperature range 5–350 K to obtain an integrated signal $I(E,m,P)$. All mass peaks at each E were recorded with unchanged MS settings (e.g., ionizer and lens voltages, pole bias, slope of the quadrupole operating line, detector high voltage). Hence, one may normalize $I(E,m,P)$ for each E and m to that of one mass, ^{12}C say. This expression is simply given by

$$\mathcal{N}(E,m,P) = \frac{I(E,m,P)}{I(E,12,P)}.$$

If one further divides this expression by the ratio of integrated TPD signals for each m acquired with the laser turned on to power P, and with the laser turned off ($P=0$), one obtains the final expression for the relative yield $\mathcal{Y}$ of species production given by

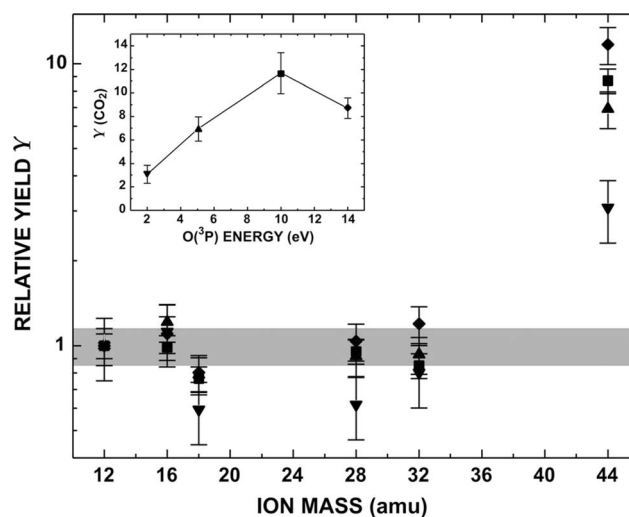$$\mathcal{Y} = \frac{N(E,m,P)}{N(E,12,P)}\frac{N(E,12,0)}{N(E,m,0)}.$$

FIG. 3. Relative production yields $\mathcal{Y}$ of the species ^{12}C, ^{16}O, $^{18}H_2O$, ^{28}CO, $^{32}O_2$, and $^{44}CO_2$ at 2 eV (▼), 5 eV (▲), 10 eV (♦), and 14 eV (■). Shown in the inset is the excitation function for production of CO_2 as a function of the $O(^3P)$ energy. The measured $\mathcal{Y}$ have not been corrected upward for dilution of the yields by background CO_2 (see text).

The usefulness of this expression lies in the fact that any mass that is *not* affected by the presence of the atom beam will give $\mathcal{Y}=1$ (i.e., no enhancement). Plotted in Fig. 3 are the measured values of $\mathcal{Y}$ for each ion mass (with the value of $\mathcal{Y}$ for ^{12}C taken as unity). The horizontal shaded band is the average value $\mathcal{Y}=0.97\pm0.1$ ($1s$) as measured for the first five masses. Also shown is the error in $\mathcal{Y}$ arising from statistical error, error in measurement of the CO pressure, and error in knowledge of the value of the laser power within the multiple-pass mirror M. In addition, a systematic bias exists in the fact that some of the observed CO_2 may be due to background CO_2 molecules that have not been exposed to the atomic beam. One can estimate this fraction from an O-atom spot diameter at the sample holder of 5 mm (obtained from trajectory estimates, and from a measured erosion pattern on a silver-mylar surface), and a sample holder diameter of 10 mm. The $\mathcal{Y}$ reported here are thus "diluted" from a true $\mathcal{Y}_t$ by the presence of the background CO_2 contribution from the entire sample holder. From geometry, one obtains at (for example) $\mathcal{Y}=3.0$ a dilution factor of 2.4, to give $\mathcal{Y}_t=7.2$. The measured yields at each energy in Fig. 3 must be considered as *lower bounds* to the true yields.

One sees a clear enhancement in $\mathcal{Y}$ for $^{44}CO_2$ by a factor of 3 at 2 eV atom energy, to a factor of 11 at 10 eV energy (results are shown in the insert separately for CO_2). This is the first direct detection of polyatomic molecule formation on a surface using superthermal atoms. Furthermore, the inset also gives a qualitative excitation function of the $\mathcal{Y}$ for CO_2. The shape of the $\mathcal{Y}$ as a function of the $O(^3P)$ energy resembles results of cross section calculations for the reactions $O(^3P)+CH_4 \rightarrow H+CH_3O$ and $OH+CH_3$; and $O(^3P)+C_2H_6 \rightarrow OH+C_2H_5$ (see, for example, Figs. 6–9 of Ref. [14]). Interestingly, CO_2 formation readily proceeds at the

lowest energy of these measurements (2 eV), and hence any barrier to the O+CO reaction must lie at $E < 2$ eV. This is consistent with results of CO_2 formation at hyperthermal O-atom energies, where $E = 0.025$ was obtained [10].

The present paper presents an unexplored channel for the study of polyatomic molecule formation on surfaces. For example, it would be interesting to study the production of methanol from CO_2, both through an oxidation channel $O+CH_4 \rightarrow CH_3OH$, and a reduction channel $4H+CO_2$ $\rightarrow CH_3OH+O$, with fast H atoms produced also from this apparatus by dissociative attachment to H_2 [21].

[1] O. Gomis, G. Leto, and G. Strazzulla, Astron. Astrophys. **420**, 405 (2004).

[2] P. A. Gerakines, M. H. Moore, and R. L. Hudson, Icarus **170**, 202 (2004).

[3] V. Mennella, M. E. Palumbo, and G. A. Baratta, Astrophys. J. **615**, 1073 (2004).

[4] M. Famá, D. A. Bahr, B. D. Teolis, and R. A. Baragiola, Nucl. Instrum. Methods Phys. Res. B **193**, 775 (2002)

[5] M. P. Bernstein *et al.*, Astrophys. J. **601**, 365 (2004).

[6] A. Schriver *et al.*, Chem. Phys. Lett. **386**, 377 (2004).

[7] P. Ehrenfreund *et al.*, Rep. Prog. Phys. **65**, 1427 (2002).

[8] K. Hiraoko *et al.*, Astrophys. J. **577**, 265 (2002).

[9] G. Vidali *et al.*, J. Geophys. Res. **109**, E07S14 (2004).

[10] J. E. Roser *et al.*, Astrophys. J. **555**, L61 (2001).

[11] M. P. Collings *et al.*, Mon. Not. R. Astron. Soc. **354**, 1133 (2004).

[12] T. Yan, W. L. Hase, and C. Doubleday, J. Chem. Phys. **120**, 9253 (2004).

[13] M. Braunstein *et al.*, J. Chem. Phys. **120**, 4316 (2004)

[14] D. Troya and G. C. Schatz, Int. Rev. Phys. Chem. **23**, 341 (2004)

[15] P. Ehrenfreund and S. B. Charnley, Annu. Rev. Astron. Astrophys. **38**, 427 (2000).

[16] D. C. B. Whittet *et al.*, Astrophys. J. **498**, L159 (1998).

[17] O. J. Orient, A. Chutjian, K. E. Martus, and E. Murad, Phys. Rev. A **48**, 427 (1993).

[18] O. J. Orient, K. E. Martus, A. Chutjian, and E. Murad, Phys. Rev. A **45**, 2998 (1992).

[19] A. S. Sandford and L. J. Allamandola, Icarus **765**, 201 (1988).

[20] H. J. Fraser, M. P. Collings, and M. R. S. McCoustra, Rev. Sci. Instrum. **73**, 2161 (2002).

[21] O. J. Orient and A. Chutjian, Phys. Rev. A **59**, 4374 (1999).